Insight - Civil Engineering 2024, 7(2), 619.
https://doi.org/10.18282/ice619

Article

Finite element modeling of the influence of FRP techniques on the seismic behavior of an arch stone bridge of historical interest

Mehdi Zekavati

Civil Engineering Department, Islamic Azad University Qazvin Branch, Nokhbegan Boulevard, Qazvin 34199-15195, Iran;
zekavati_mehdi@yahoo.com

CITATION

Zekavati M. Finite element modeling of the influence of FRP techniques on the seismic behavior of an arch stone bridge of historical interest. Insight - Civil Engineering. 2024; 7(2): 619. https://doi.org/10.18282/ice619

ARTICLE INFO

Received: 27 May 2024
Accepted: 15 August 2024
Available online: 8 November 2024

Abstract: In this paper, a masonry bridge is simulated in order to assess both its structural and seismic vulnerability. Therefore, the present study aimed to approximately analyze the real behavior of Mikron Bridge structure. The modeling was conducted by combining the finite element method (FEM) and discrete element method (DEM) using the ABAQUS® software. By comparing the results of numerical and experimental modal analyses, the accuracy of simulation was verified. To simulate the seismic behavior of the Mikron Bridge, the component of Erzincan earthquake occurred in 1992 was used. The results extracted from the seismic analysis show that some parts of the bridge structure are damaged but not destroyed.

Keywords: discrete element method; bridge; finite element method; simulation; masonry; ABAQUS; dynamic loads

1. Introduction

The stone arch bridges have a different dimension, span, and building style. Since some of them date back to 2000 years ago, they are important components of the cultural heritage [1–3]. Stone arch bridges are still widely used in the railway system of European countries such as Italy, England, France, Spain, and Germany. The European railway was built in a century and the first railway in Italy was built in 1839 where a number of bridges were built between 1860 and 1910 [4]. Stone bridges are among the oldest architectural structures, some of which are over 100 years old [3,5]. Today, in many countries, stone bridges are considered among the effective elements in the railway and road networks [6]. Several modeling approaches for masonry structures (Continuous and Discontinuous Modeling) Currently Being developed by several research teams Bridge arch models are provided for study [7].

The failure behavior of stone structures can be explored using the finite element analysis [8,9]. Referring to the conducted research, three modeling approaches are suggested for stone structures: (1) discrete method, (2) continuous method, and (3) combination of discrete and continuous methods [10]. The NSCD algorithm allows modeling the behavior of granular materials by the friction between the blocks with a rigid or mechanical behavior. One advantage of the combined NSCD method is that there is no need for artificial damping for the stability of stone structure [11]. The behavior of stone bridge can be simulated using numerical approaches such as finite element method (FEM) and discrete element method (DEM). These simulation techniques allow the bearing capacity to be calculated under the traffic load [12,13]. The maintenance and restoration of historic structures are among the major interests of many researchers [14,15].

Structure reinforcement by FRP has gained considerable attention in recent

years. Application of FRP will lead to an increase in the hardness and strength of the structure. Rock panel retrofit by CFRP composite will lead to its enhanced hardness [16]. FRP-assisted retrofit prevents the early fracture and increases the strength of stone structures [17]. Moreover, reinforcement of parabolic stone arch by FRP results in an increase of power [18]. Recently, FRP has been employed for reinforcement of stone structures. In this regard, retrofit by FRP has resulted in enhancement of compressive strength in stone buildings. Although this technique has proved to be quite effective, various drawbacks arise when organic resins are used to bind fibres [19]. For instance, application of FRP ribbon for stone wall reinforcement has resulted in a decrease in out-planes deviation [20].

In France, a new and reliable seismic design was prop A comparative study has been carried out on the global behavior and local mechanisms and in particular emphasizes that mechanical anchor systems play an important role in improving the behavior of reinforced walls (by FRP and TRC) and that retrofitting solutions by TRC allow. Improving ductility of walls with lower strength compared to FRP solutions [21].

Arch reinforcement by FRP causes two important consequences: 1—an increase in stone arch capacity and 2—a reduction in a lateral drift in the stone arch [22]. Regarding the empirical results, after installation of FRP ribbon to building a wall, improvement in seismic and plasticity was observed [23]. Results of empirical studies indicated that stone column reinforcement by FRP leads to a decrease in crack propagation, leading to substantial increase in the load capacity of column [24]. One of the challenges for researchers in this study was to accurately simulate the structural behavior of stone bridge under the earthquake load, which provides the scientific and engineering communities with a clear and real insight regarding the behavior of the bridge structure. In the present study, the numerical modeling of stone bridge structure is done using a combination of FEM and DEM approaches Seismic behavior of mikron stone bridge was addressed in this study. A combination of FEM and DEM was employed for getting closer to the real behavior of the bridge. One of the unique features of this combinational method is simulation close to reality. Modal numerical analysis was also used to verify the modeling.

2. Behavioral model of contact between elements

In the analysis of solids, a special situation occurs in places where discontinuous behavior occurs between two finite elements. Between elements with dissimilar materials, between blocks, connections and material failure causes this special situation. The stiffness matrix of contact elements is assembled in the usual way.

$$k^e a^e = F^e \tag{1}$$

where k^e is the stiffness matrix of the contact elements and a^e is the displacement vector of the double nodes in the intermediate elements and F^e is the force vector.

$$K^e = \int_A B^T DBdA \tag{2}$$

$$D = \begin{bmatrix} k_{s1} & 0 & 0 \\ 0 & k_{s2} & 0 \\ 0 & 0 & k_n \end{bmatrix} \tag{3}$$

$$a^e = \begin{Bmatrix} a_1 \\ \cdot \\ a_n \end{Bmatrix}, \; a_i = \begin{Bmatrix} u_i \\ v_i \\ w_i \end{Bmatrix} \tag{4}$$

Matrix B relates the displacement vector of the nodes to the relative vector. To define the non-linear behavior of the contact surfaces and separations, the connection plane must be properly described. For the contact surface without tensile resistance, when the normal force of the contact surface becomes tensile. happens. The submission function is described as follows.

$$F_n = t_n \tag{5}$$

$F_n$is the normal force vector of the contact surface t_n is the surface contact pressure.

$$t_n = k_n \delta_n \tag{6}$$

δ_nThe displacement is relative. Tensile strength can be defined for the contact surface.

$$F_n = t_n - T \tag{7}$$

With increasing shear strength, irreversible sliding occurs. We will have the Mohr-Coulomb yield function.

$$F_s = t_s + S \tag{8}$$

$$t_{si} = k_{si} \delta_{si}, i = 1,2 \tag{9}$$

F_s is the tangential force vector at the contact surface δ_{si} Relative displacement along the tangent line and t_{si} is the shear force.

$$t_s = \sqrt{t_{s1}^2 + t_{s2}^2} \tag{10}$$

$$S = t_n \tan \varphi \tag{11}$$

Different methods can be used to apply the above constraints. We can refer to the penalty method and the generalized Lagrange method. The Lagrange coefficients increase the solution time, but avoid numerical errors resulting from unfavorable numerical conditions in high difficulties. In the penalty method, the contact force is proportional to the amount of penetration. In the penalty method, numerical softening occurs, which reduces the binding of the contact and prevents repeated solving. The penalty method can cover relation (6) both linearly and non-linearly. In the linear penalty method, the relationship between penetration and pressure is linear. In the non-linear penalty method, the increase in hardness is within the range of the lowest constant initial hardness and the highest constant final hardness (**Figure 1**).

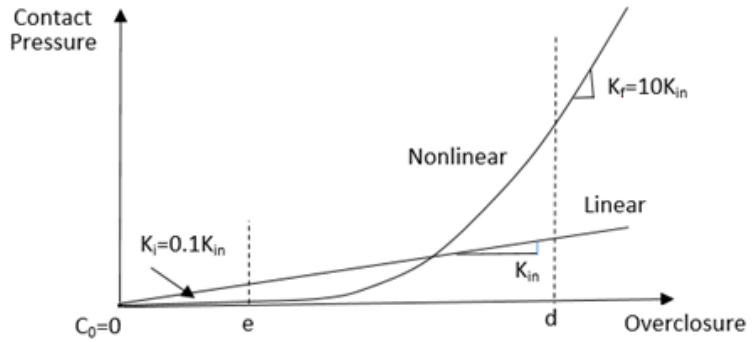

Figure 1. Linear and non-linear relationship of influence.

The non-linear penalty mode has four specific ranges (**Figure 2**).

1) Inactive contact range: In this range, the contact pressure remains zero.

2) Fixed Initial Penalty Hardness Range: The contact pressure changes linearly in the range of $-C_0$ to e.

3) Hardening range: The contact pressure changes non-linearly in the range e to d.

4) Fixed Final Penalty Hardness Range: The contact pressure changes linearly for values larger than d.

The ranges mentioned above can be changed taking into account the purpose of using the contact elements. The low initial hardness has caused the repetitions to converge in Newton's method. Due to the high final hardness, penetration has been kept at an acceptable level for the contact pressure. Therefore, it is clear that this modeling method is close to reality.

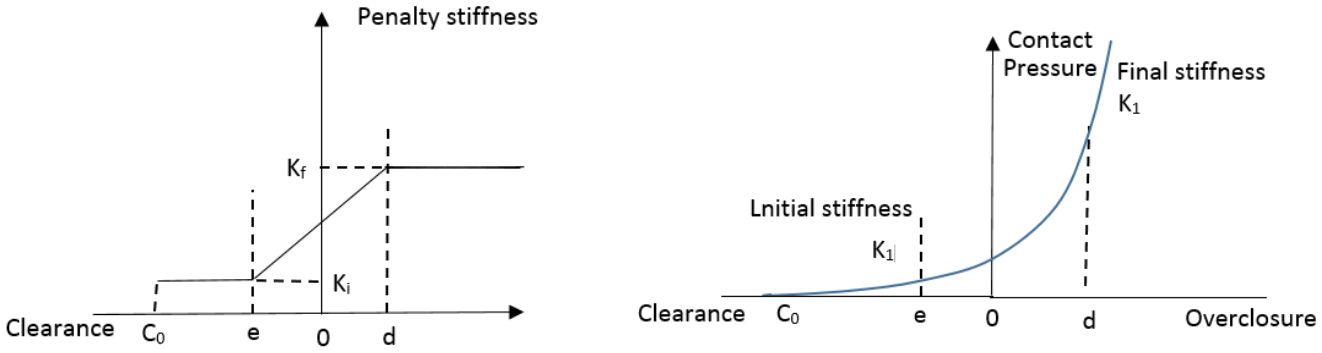

(a) **(b)**

Figure 2. The non-linear relationship of penalty: **(a)** fixed initial penalty hardness range; **(b)** fixed final penalty hardness range.

The main purpose of using the non-linear penalty method is to create uniformity in the opening of the seams and timely opening of the seams. The values of the mentioned ranges should be chosen in such a way that the modeling is close to reality. According to the following relations can be the result found that k_s depends only on the coefficient of friction and the maximum amount of elastic slip, δ_{scrit}

$$t_s = \mu t_n \tag{12}$$

where μ is the friction coefficient corresponding to $\tan\varphi$. t_n is the contact normal

force.

$$k_s = \frac{t_s}{\delta_{scrit}} \tag{13}$$

δ_{scrit} is the maximum elastic slip.

3. Geometry of stone arch Mikron Bridge

After the restoration, the Mikron stone bridge has a circular arch formed by two internal and external stone arches with a thickness of 0.5m and 0.15m. Also, the sizes of the side walls and timber block are 0.5m and 2m, respectively. The total lengths of the bridge and its arch are 33.80 and 19.49m respectively (**Figures 3**–**5**). As also presented in **Table 1**, in this study, By using penalty method, the coefficients of friction between the stones and coefficient of friction between the stones and mortars were 0.7. All materials were modeled using Drucker–Prager failure criterion model (**Table 1** and **Figure 6**). In this study, the bridge was analyzed under seismic and dead load, in presence and absence of FRP. All surfaces of the arch and spandrel wall were retrofitted using FRP, and the interaction between FRP and surface of stones was analyzed using solid shell coupling. Specifications of FRP are provided in **Table 2** in finite element model all degrees of freedom at boundary conditions in of the bridge are considered fixed. **Figure 8** discrete element model created in ABAQUS **Figure 7**.

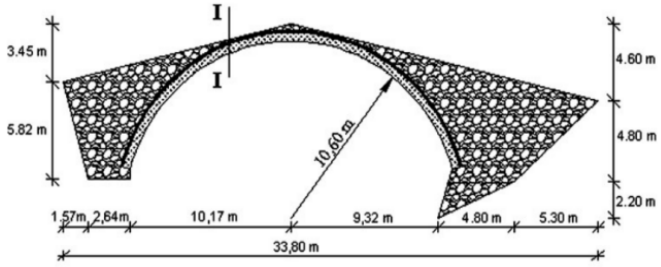

Figure 3. The plan view of the bridge [25].

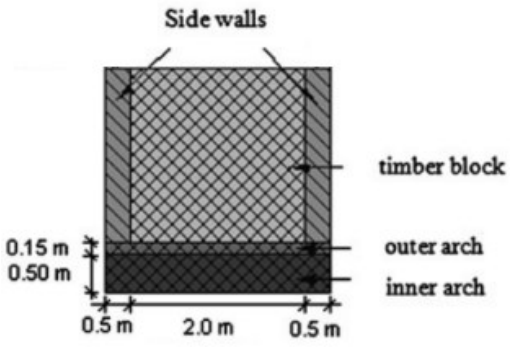

Figure 4. Geometry dimensions of Mikron Bridge [25].

Figure 5. View of the stone bridge Mikron.

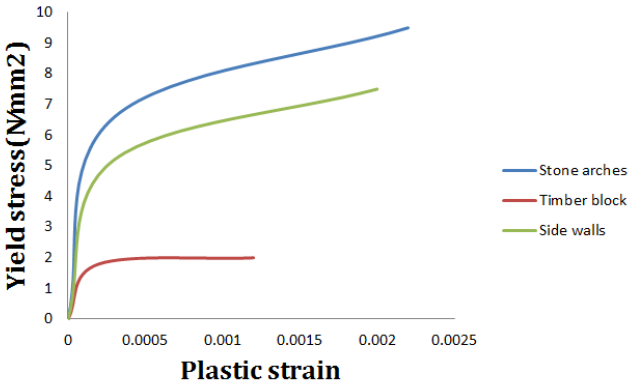

Figure 6. Mechanical material property.

Table 1. Mechanical material property.

Material	Modulus of elasticity (N/mm^2)	Poisson ratio	Cohesion (N/mm^2)	Friction Angle (°)	Density (kg/m^3)	Compressive yield stress (N/mm^2)	Dilation Angle (°)
Stone arches	3000	0.2	1.2	50	1600	6.6	35
Side walls	2500	0.2	1	48	1400	5.2	32
Timber block	1500	0.05	0.5	32	1300	1.8	17

Table 2. Mechanical material property.

Material	Modulus of elasticity (N/mm2)	Poisson ratio	Ten stress Fiber dir. (N/mm2)	Com stress Fiber dir.	Ten stress Transv dri. (N/mm2)	Com stress Transv dri.	Shear strength	Cross-prod Term coeff	Stress Limit (N/mm2)
FRP	22000	0.3	120	0.3	120	0.3	0.3	0	120

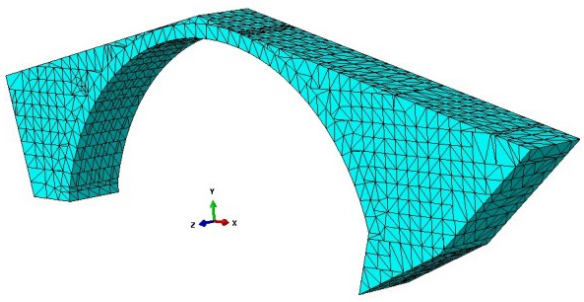

Figure 7. FE model.

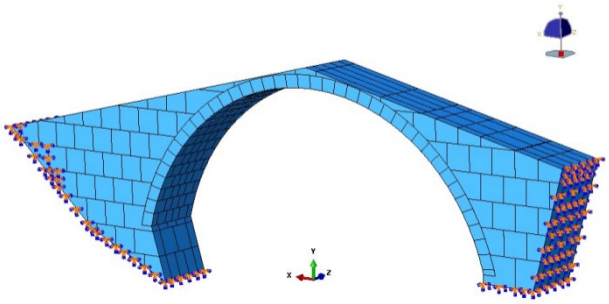

Figure 8. Boundary conditions.

4. FEM calibration of the Mikron Arch Bridge

The Mikron bridge is made of three structural parts: side walls, stone arches, and timber block. In this study, to make the behavior of numerical modeling closer to the natural behavior of the bridge structure, a hybrid FEM/DEM method is applied. The friction is defined between the contact area of blocks. The friction coefficient of 0.7 is used for the block contact areas. One of the challenges authors faced with is to ensure the accuracy of the simulation. Therefore, in the present study, the numerical model is calibrated through the experimental modal analysis. The natural frequencies of the bridge are obtained from two experimental methods of SSI and EFDD [25]. The natural frequencies obtained from the experimental analysis range from 6.063 to 13.59 Hz. A total of 18,460 elements of C3D10 are used for modal analysis. The C3D10 element has 10 quadratic tetrahedral nodes. From the results of the numerical modal analysis, the range of four frequencies is between 5.9441Hz and 13.500Hz (**Figure 9**). The distance between the results of experimental and numerical analyses is about 2% (**Table 3**). As a result, the distance between the frequency obtained from FEM and that extracted from the experimental method is almost negligible. During the calibrated FEM and DEM analysis, Rayleigh damping coefficients are calculated for a 1.945% damping ratio as obtained from ambient vibration tests (**Table 3**).

Table 3. Analytical and experimental natural frequencies of the mikron Arch Bridge after model calibration.

Mode number	Calibrated analytical frequencies (Hz)	Experimental frequencies (Hz)		Experimental damping ratios (%)		Max difference After calibration
		EFDD	SSI	EFDD	SSI	
1	5.9441	6.063	6.065	1.945	1.855	2%
2	9.5512	9.563	9.558	0.967	0.923	0.07%
3	10.345	9.906	10.180	0.835	0.815	1.7%
4	13.500	13.590	13.590	0.258	0.289	0.6%

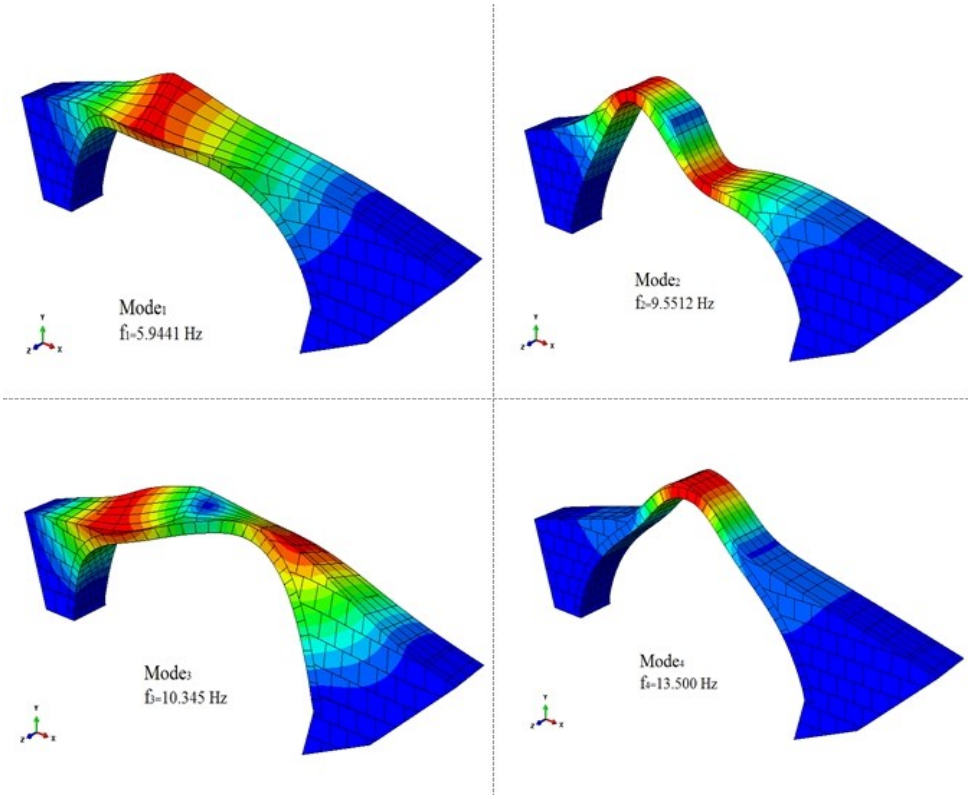

Figure 9. Four mode calibrated frequencies of the mikron Arch Bridge.

5. Seismic analysis of Mikron Arch Bridge

5.1. Earthquake

The data used in this study are from the Erzincan earthquake occurred in 1992. The maximum acceleration of Erzincan earthquake is approximately 0.486g and the largest earthquake displacement occurred in 5 s equals to 0.2 m. It has to be noted that the three component of earthquakes is used in this work (**Figures 10**–**13**). The earthquake occurred in the North Anatolian Fault, which is the nearest fault to the Mikron Arch Bridge that were the subject of this work.

5.2. Seismic behaviors of Mikron Arch Bridges

The accurate simulation of the seismic behavior of stone structures is a major challenge for the research communities. Therefore, due to the complex geometry and nonlinear behavior of the materials, the simulation of historic structures is very difficult. Some measures are taken to accurately assess the seismic behavior of the historic stone structures for preserving such important structures. Thus, the present study aimed to simulate an accurate behavior of stone structures. Accordingly, calibrating the FEM is a critical issue. In this study, a combination of FEM and DEM approaches is used to simulate the damages incurred to the structure of Mikron Bridge. By combining the FEM and DEM approaches, it is possible to simulate the cracks, damages, and destructions. In the numerical modeling, 18,460 elements of C3D10M are used with a 10-node modified quadratic tetrahedron. Some cracks appeared on the side wall of the bridge 3.8 s after the earthquake; and after 7.6 s, the side-wall cracks were made larger. The stone arch cracks were increased in 5.3 s, but no part of the

bridge structure was collapsed or destroyed (**Figure 14**). Some of the blocks of the side wall and arch bridges are numbered in **Figure 15**. The blocks started to move 2.8 s after the earthquake in the Z direction, and the maximum displacement was caused 5.5 s later (**Figure 16**). The maximum displacement occurred between 3.5 s and 7.6 s in the Y direction which is 0.03 m (**Figure 17**). The cracks in the arch appeared 3 s after the earthquake; and after 5.5 s, they reached their maximum size (**Figure 18**). The maximum value of crack occurred between 3.5 s and 7.6 s (**Figure 19**). From the results extracted from the FEM analysis, it is seen that the bridge is not destroyed, but some parts of its structure are damaged. Due to the higher hardness in the Y direction compared to the Z direction in Mikron bridge, the movement of stones in the Z direction is more than the movement of stones in the Y direction.

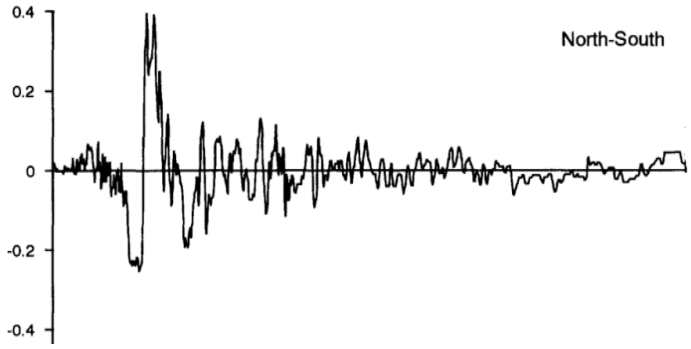

Figure 10. Seismic acceleration North-South.

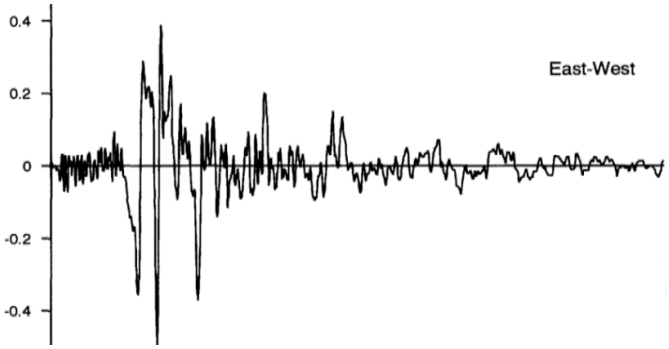

Figure 11. Seismic acceleration East-West.

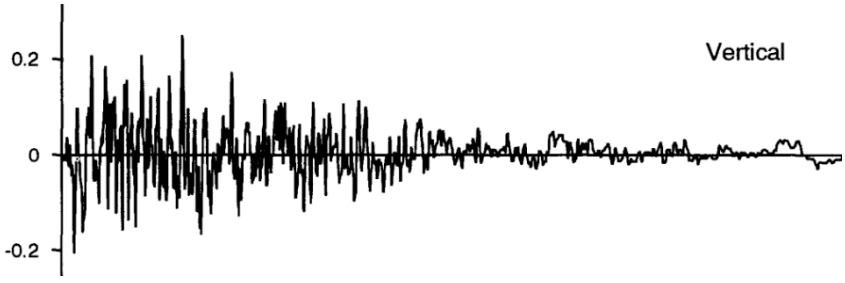

Figure 12. Seismic acceleration Vertical.

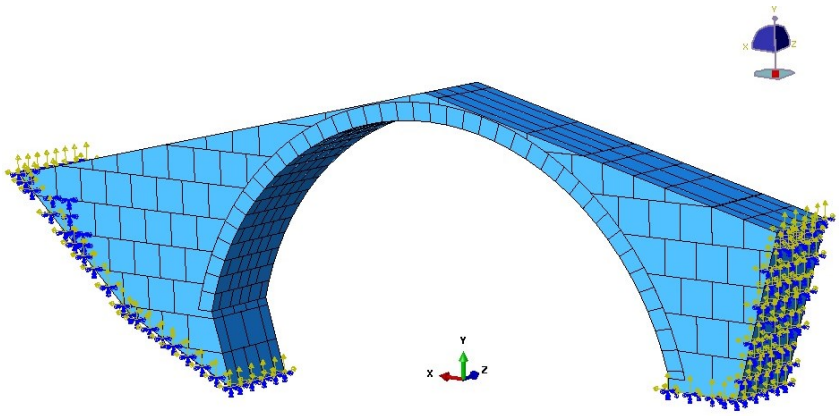

Figure 13. Boundary conditions.

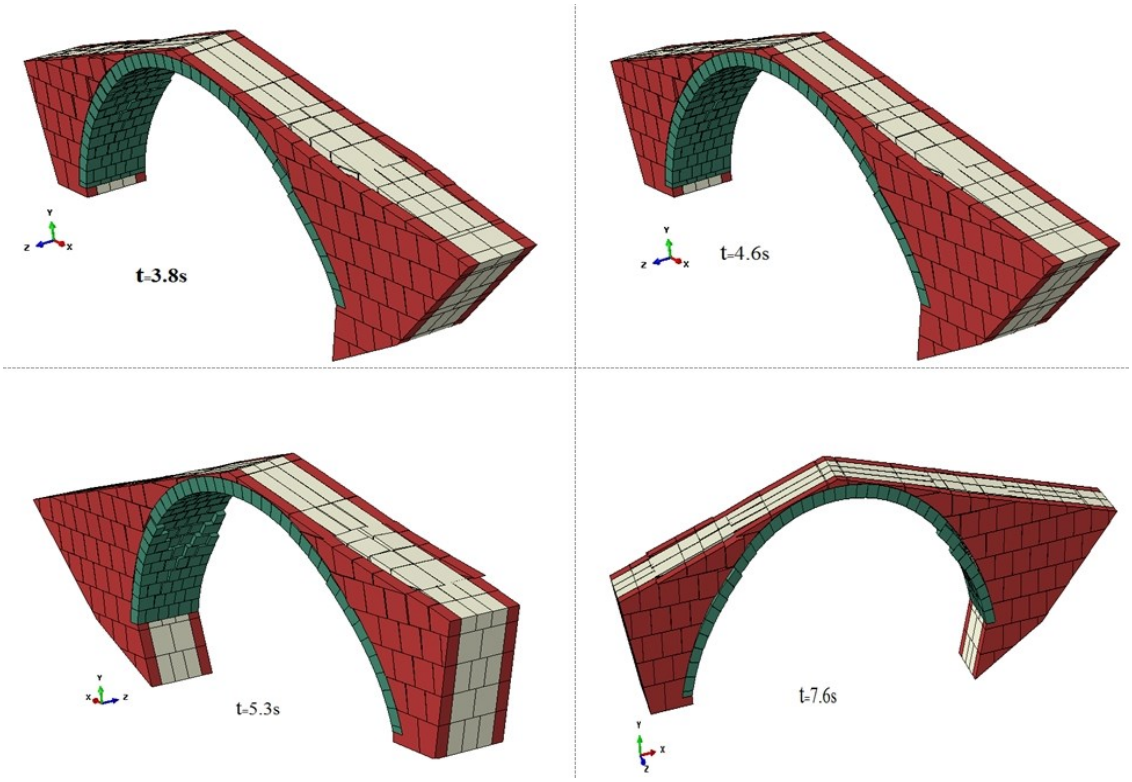

Figure 14. Bridge deformation after the earthquake the past time.

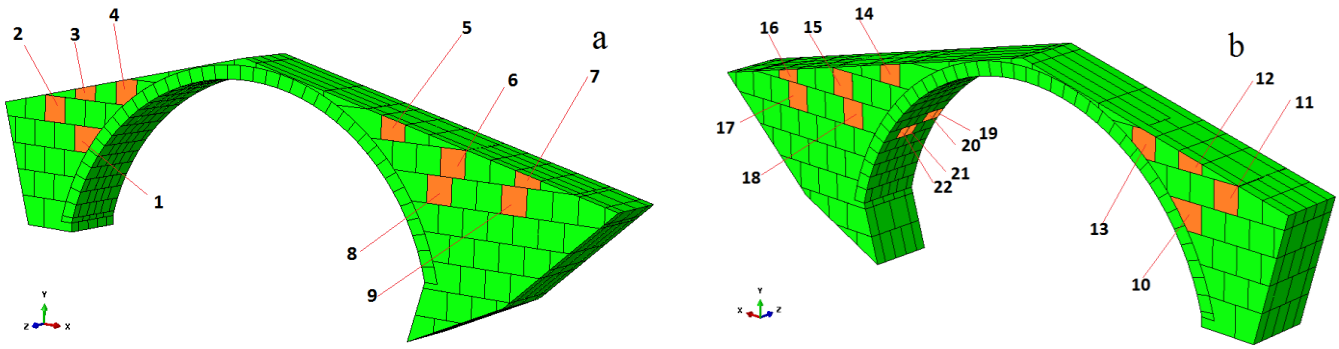

(a) **(b)**

Figure 15. Numbering block of finite element model: **(a)** right wall; **(b)** left wall.

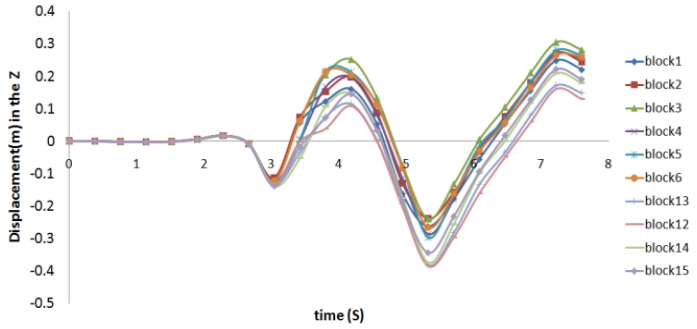

Figure 16. Displacement (m) in the Z direction of the wall of bridge.

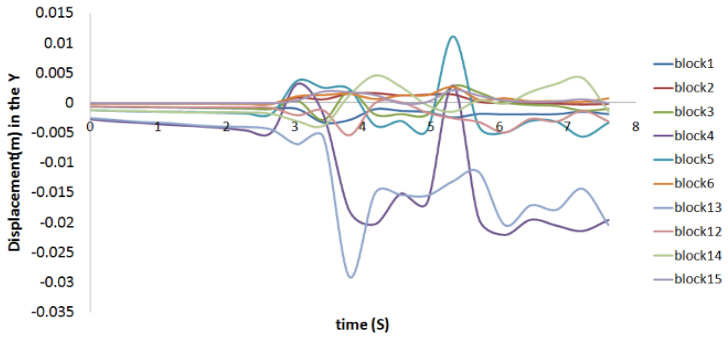

Figure 17. Displacement (m) in the Y direction of the wall of bridge.

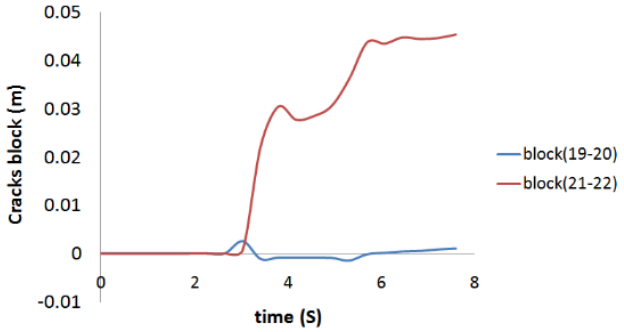

Figure 18. Cracks (m) between the blocks.

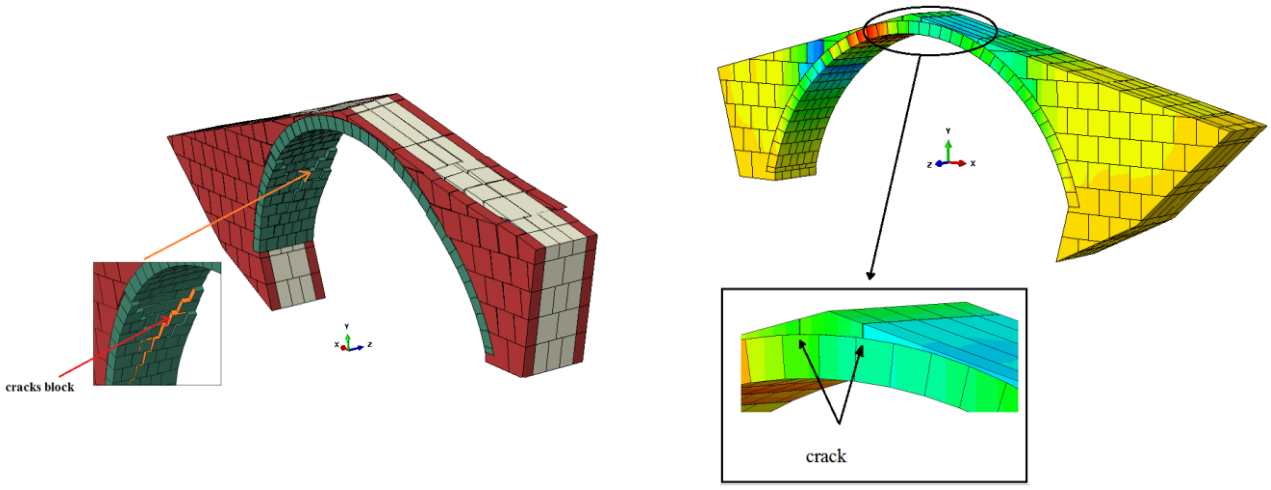

(a) **(b)**

Figure 19. Expansion of cracks in the bridge: **(a)** Crack in the arch; **(b)** Crack in the wall.

5.3. Retrofitting Mikron arch bridge using FRP in the horizontal direction

According to the analysis results of the Mikron Bridge, some large cracks are created in the arch bridge and cause damage to the bridge structure. Therefore, in this study, the authors decided to reduce the bridge damages using a retrofitting method. One of the considered methods is to retrofit the bridge arch using the FRP in the horizontal direction. The thickness of 1 mm was used for FRP while the S4R element was used for modeling the FRP. The Contact between blocks and FRP was selected as "shell-to-solid couplings". Retrofitting caused reducing the displacement of side-wall blocks in the Z direction, with the maximum displacement being about 0.35 m (**Figure 20**). This type of retrofitting had no effect on the displacement of the blocks in the Y direction compared to that before the retrofitting (**Figure 21**). The arch cracks in this method are greatly reduced compared to those before the retrofitting and the largest crack is about 6 mm (**Figure 22**). After 3.8 s, the displacement of the blocks was started and reached its peak in 5.3 s. Then, 7.6s after the earthquake, the displacements were decreased (**Figure 23**). Retrofitting by bonding FRP in the horizontal direction substantially reduced the cracks, and the displacement of the blocks in the Z and Y directions was decreased compared to before the retrofitting.

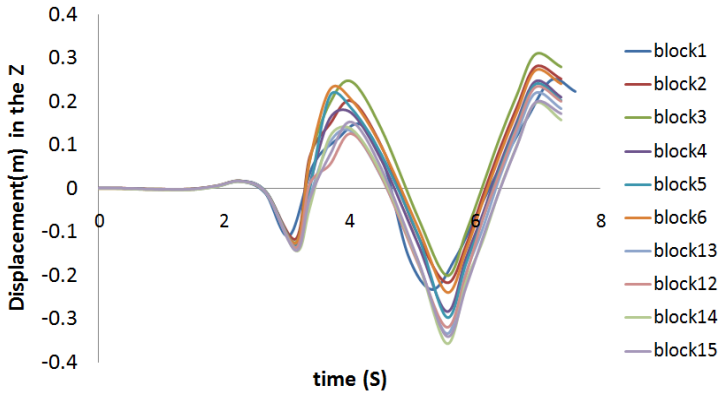

Figure 20. Displacement (m) in the Z direction of the wall of bridge (FRP in the horizontal direction).

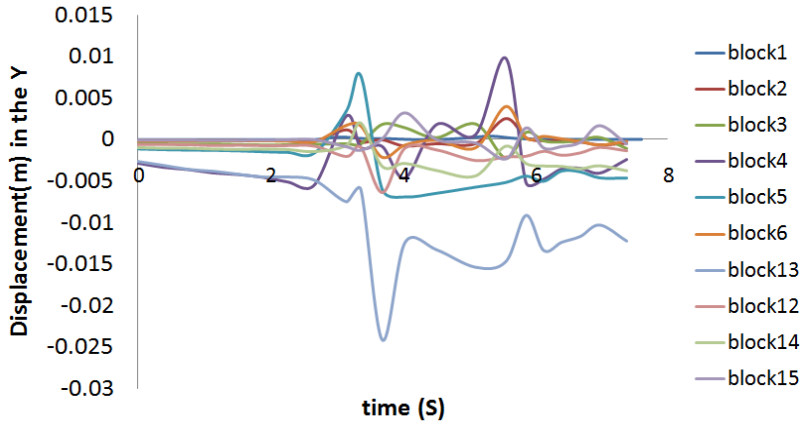

Figure 21. Displacement (m) in the Y direction of the wall of bridge (FRP in the horizontal direction).

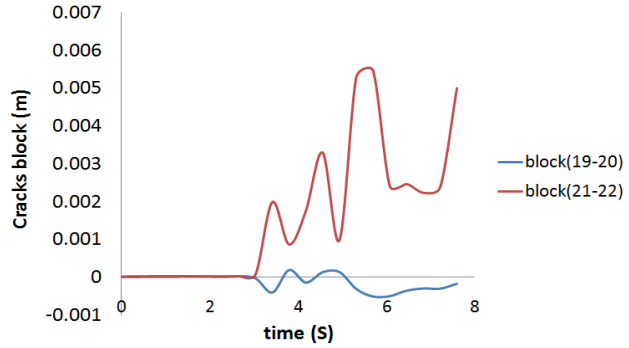

Figure 22. Cracks (m) between the blocks (FRP in the horizontal direction).

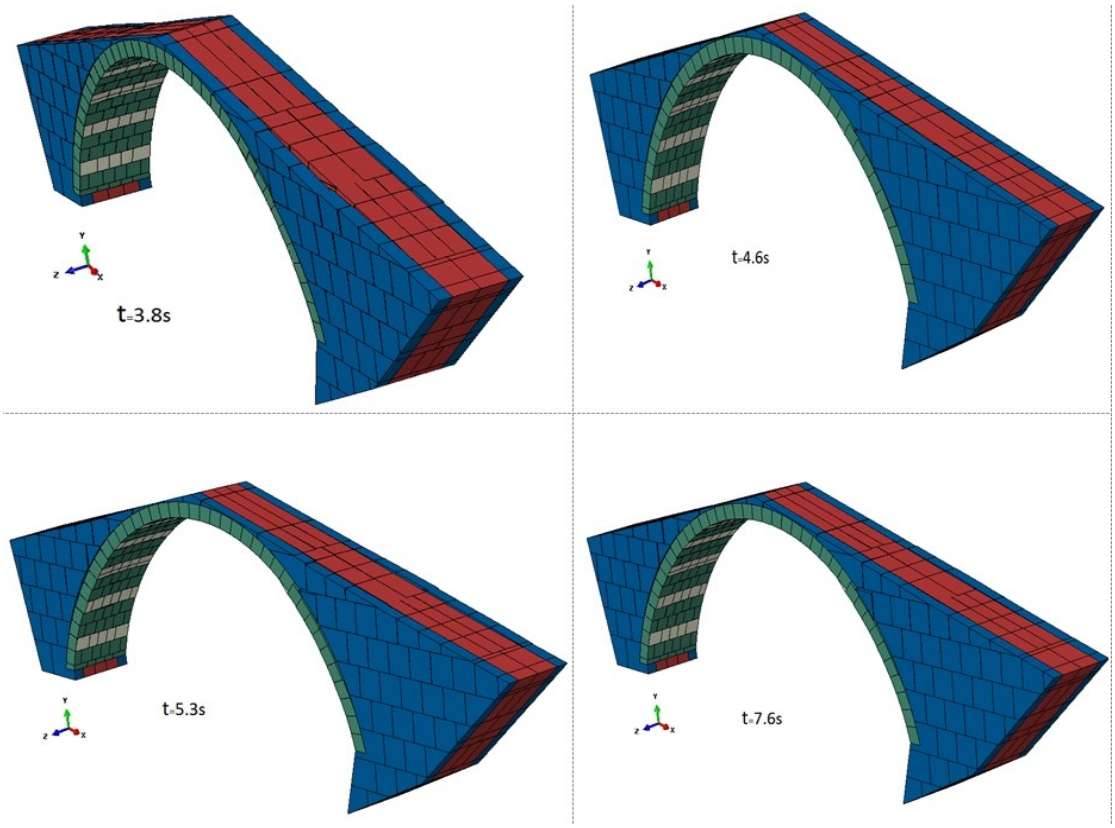

Figure 23. Bridge deformation after the earthquake the past time (FRP in the horizontal direction).

5.4. Retrofitting Mikron arch bridge using FRP in the vertical direction

One way for retrofitting the Mikron Bridge is to bond FRP to the arch in the vertical direction. In this method, the surface of the stone arch is retrofitted using 3 FRPs with all features of FRP being considered as before. According to the analysis results, the obtained structure had no effect on the displacement of the blocks in the Z direction compared to the stated before the retrofitting; and at most it reached 0.42 m (**Figure 24**). The block displacements were increased in the Y direction, where the maximum displacement was 3 cm (**Figure 25**). The cracks in the arch were decreased compared to before the retrofitting and the largest crack was 2.8 cm, which is (**Figure 26**). After 3.8 s, the displacement of the blocks was started and reached its peak in 5.3 s; and 7.6s after the earthquake, the arch cracks were increased (**Figure 27**).

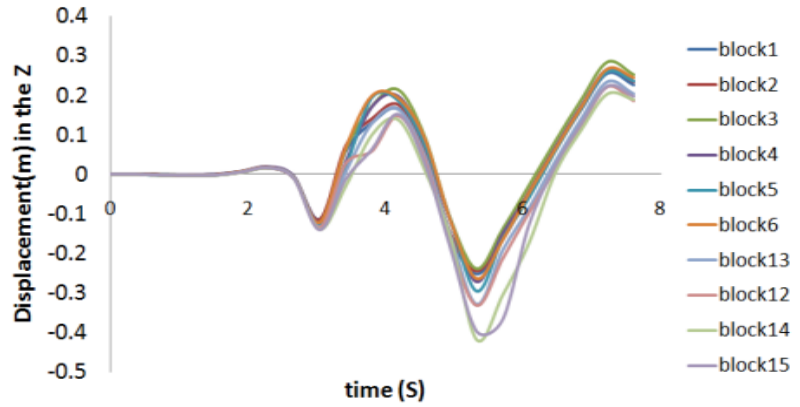

Figure 24. Displacement(m) in the Z direction of the wall of bridge (FRP in the vertical direction).

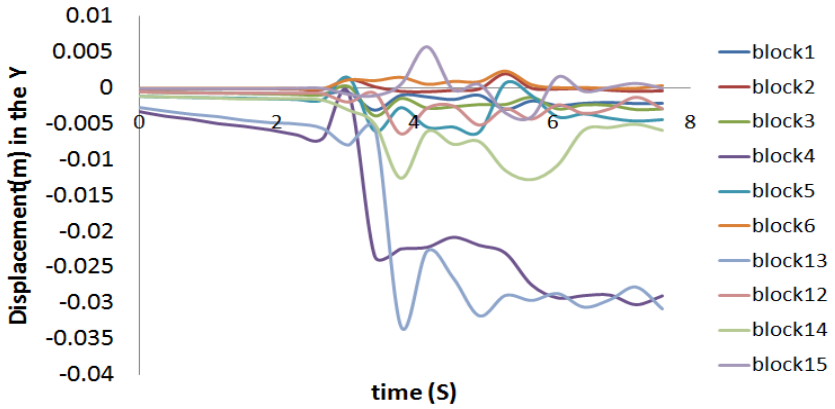

Figure 25. Displacement(m) in the Y direction of the wall of bridge (FRP in the vertical direction).

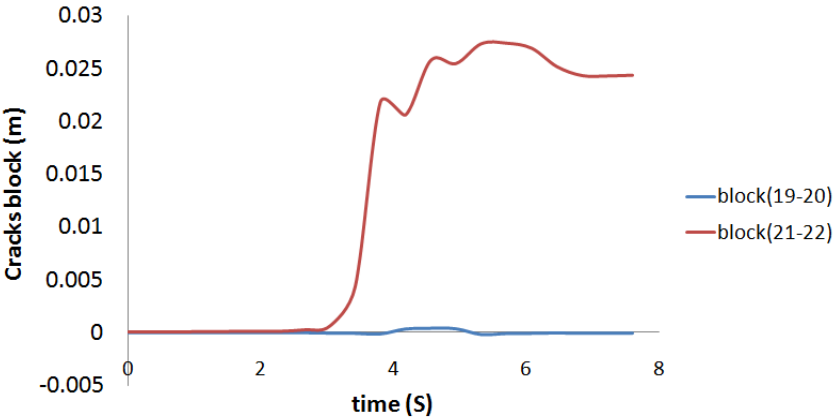

Figure 26. Cracks (m) between the blocks (FRP in the vertical direction).

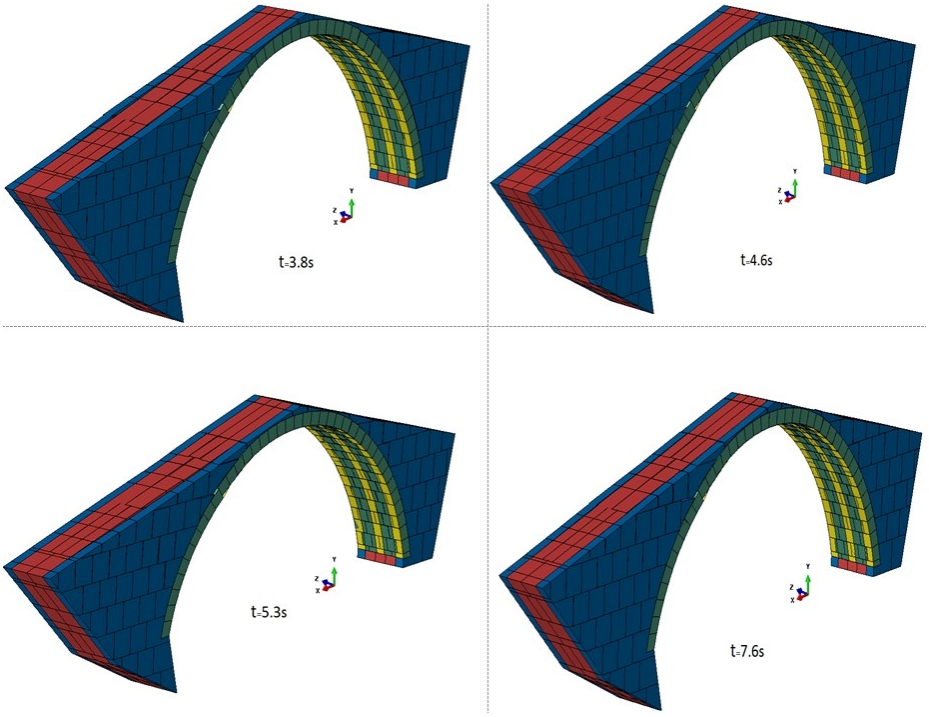

Figure 27. Bridge deformation after the earthquake the past time (FRP in the vertical direction).

6. Conclusions

The present study was conducted to simulate the exact behavior of the Mikron bridge structure. The accurate knowledge of the behavior of structures helps advance the goals of researchers to preserve the structures. These goals can be achieved using data obtained from the experimental analysis. The main results of the present work are outlined as follows:

1) A combination of finite element method (FEM) and discrete element method (DEM) was used for simulation. The difference in modal analysis results obtained from the calibration of the discrete model with experimental methods of EFDD and SSI reached about 2%.
2) Using the combined method to simulate the seismic behavior of the bridge makes it possible for engineers to model the damage caused by the earthquake. Therefore, the Mikron Bridge was modeled by combining the FEM and DEM approaches to simulate the cracks created by the earthquake in the structure.
3) The maximum displacement in the Z direction was 0.4 m that occurred after 5.5 s while the maximum displacement in the Y direction was 0.03 m that occurred between 3.5 s and 7.6 s. Also, the largest crack (equal to 0.045 m) occurred between 3.5 s and 7.6 s. From the results extracted from the FEM analysis, it is seen that some parts of the bridge structure are damaged, but the bridge is not destroyed.
4) Retrofitting by bonding FRP in the horizontal direction substantially reduced the cracks, and the displacement of the blocks in the Z and Y directions was decreased compared to before the retrofitting.
5) Retrofitting by bonding FRP in the vertical direction had no significant impact on the displacement of blocks in the Z and Y directions compared to the state

before the retrofitting, and the cracks were reduced compared to before the retrofitting. According to these results and by comparing the results with each other, retrofitting by bonding FRP in the horizontal direction provided the best seismic response compared to bonding FRP in the vertical direction.

6) By comparing the results of two retrofitting methods, it can be found that by changing the direction of FRP the results also changed. Finally, bonding FRP in the horizontal direction provided the best performance and reduced the arch cracks.

The simultaneous use of two methods FEM and DEM for modeling the dynamic behavior of masonry structures increases the accuracy of the results. It is suggested to model the building structures that are damaged by the earthquake with the FEM and DEM method in future studies. The high accuracy of this method can help researchers to correctly understand the behavior of masonry structures. As a result, they can use appropriate methods to protect structures against earthquakes.

FRP in the vertical direction increases the bending capacity of the bridge arch, but it does not reduce the horizontal cracks in the bridge arch. Due to the low stiffness of the bridge in the Z direction, which increases the movement of stones in this direction, therefore FRP Vertical is not suitable for reducing cracks in horizontal direction. As a result, horizontal FRP has been used to reduce cracks in the Z direction.

Conflict of interest: The author declares no conflict of interest.

References

1. Altunisik AC., Bayraktar A, Genc AF. A study on seismic behaviour of masonry mosques after restoration. Earthquakes and Structures. 2016; 10(6): 1331–1346.
2. Mamaghani IHP. Analysis of Masonry Bridges. Transportation Research Record: Journal of the Transportation Research Board. 2006; 1976(1): 13–19. doi: 10.1177/0361198106197600102
3. Catalan RO, Aldea LE. New Tendencies on Repair and Strengthening on Masonry Arch Bridges. In: Proceedings of the 5th International Conference on Arch Bridges; 2007; pp. 719–724.
4. Reccia E, Milani G, Cecchi A, et al. Full 3D homogenization approach to investigate the behavior of masonry arch bridges: The Venice trans-lagoon Railway Bridge. Construction and Building Materials. 2014; 66: 567–586. doi: 10.1016/j.conbuildmat.2014.05.096
5. Cakir F, Burcin SS. Structural Performance of Renovated Masonry Low Bridge in Amasya, Turkey. Earthquakes and Structures. 2016: 8(6): 1387–1406.
6. Pelà L, Aprile A, Benedetti A. Seismic assessment of masonry arch bridges. Engineering Structures. 2009; 31(8): 1777–1788. doi: 10.1016/j.engstruct.2009.02.012
7. Idris J, Verdel T, Al-Heib M. Numerical modelling and mechanical behaviour analysis of ancient tunnel masonry structures. Tunnelling and Underground Space Technology. 2008; 23(3): 251–263. doi: 10.1016/j.tust.2007.04.006
8. Orduña A, Lourenço PB. Three-dimensional limit analysis of rigid blocks assemblages. Part II: Load-path following solution procedure and validation. International Journal of Solids and Structures. 2005; 42(18-19): 5161–5180. doi: 10.1016/j.ijsolstr.2005.02.011
9. Daniel, Oliveira V. Experimental and numerical analysis of blocky masonry structures under cyclic loading (Portuguese). Available online: https://repositorium.sdum.uminho.pt/handle/1822/180 (accessed on 3 March 2024).
10. Jing, L. A Review of Techniques, Advances and Outstanding Issues in Numerical Modelling for Rock Mechanics and Rock Engineering. International Journal of Rock Mechanics and Mining Sciences. 2003; 40(3): 283–353.
11. Rafiee A, Vinches M, Bohatier C. Application of the NSCD method to analyse the dynamic behaviour of stone arched structures. International Journal of Solids and Structures. 2008; 45(25-26): 6269–6283. doi: 10.1016/j.ijsolstr.2008.07.034
12. Costa C, Arêde A, Morais M, et al. Detailed FE and DE Modelling of Stone Masonry Arch Bridges for the Assessment of

Load-carrying Capacity. Procedia Engineering. 2015; 114: 854–861. doi: 10.1016/j.proeng.2015.08.039
13. Pulatsu B, Bretas EM, Lourenco PB. Discrete element modeling of masonry structures: Validation and application. Earthquakes and Structures. 2016; 11(4): 563–582.
14. Lourenço PB, Krakowiak KJ, Fernandes FM, et al. Failure analysis of Monastery of Jerónimos, Lisbon: How to learn from sophisticated numerical models. Engineering Failure Analysis. 2007; 14(2): 280–300. doi: 10.1016/j.engfailanal.2006.02.002
15. Rovithis EN, Kyriazis DP. Seismic Assessment and Retrofitting Measures of a Historic Stone Masonry Bridge. Earthquake and Structures. 2016; 10(3): 645–667.
16. Saghafi MH, Safakhah S, Kheyroddin A, et al. In-plane Shear Behavior of FRP Strengthened Masonry Walls. APCBEE Procedia. 2014; 9: 264–268. doi: 10.1016/j.apcbee.2014.01.047
17. Ascione L, Feo L, Fraternali F. Load carrying capacity of 2D FRP/strengthened masonry structures. Composites Part B: Engineering. 2005; 36(8): 619–626. doi: 10.1016/j.compositesb.2004.12.004
18. Bertolesi E, Milani G, Fedele R. Fast and reliable non-linear heterogeneous FE approach for the analysis of FRP-reinforced masonry arches. Composites Part B: Engineering. 2016; 88: 189–200. doi: 10.1016/j.compositesb.2015.11.005
19. Fossetti M, Minafò G. Comparative experimental analysis on the compressive behaviour of masonry columns strengthened by FRP, BFRCM or steel wires. Composites Part B: Engineering. 2017; 112: 112–124. doi: 10.1016/j.compositesb.2016.12.048
20. Hamed E, Rabinovitch O. Out-of-plane behavior of unreinforced masonry walls strengthened with FRP strips. Composites Science and Technology. 2007; 67(3-4): 489–500. doi: 10.1016/j.compscitech.2006.08.021
21. Bui TL, Si Larbi A, Reboul N, et al. Shear behaviour of masonry walls strengthened by external bonded FRP and TRC. Composite Structures. 2015; 132: 923–932. doi: 10.1016/j.compstruct.2015.06.057
22. De Lorenzis L, Dimitri R, La Tegola A. Reduction of the lateral thrust of masonry arches and vaults with FRP composites. Construction and Building Materials. 2007; 21(7): 1415–1430. doi: 10.1016/j.conbuildmat.2006.07.009
23. Zhang S, Yang D, Sheng Y, et al. Numerical modelling of FRP-reinforced masonry walls under in-plane seismic loading. Construction and Building Materials. 2017; 134: 649–663. doi: 10.1016/j.conbuildmat.2016.12.091
24. Witzany J, Cejka T, Zigler R. Problems of Masonry Strengthening with Carbon- and Glass Fibre Fabric. Procedia Engineering. 2011; 14: 2086–2093. doi: 10.1016/j.proeng.2011.07.262
25. Sevim B, Bayraktar A, Altunişik AC, et al. Assessment of nonlinear seismic performance of a restored historical arch bridge using ambient vibrations. Nonlinear Dynamics. 2010; 63(4): 755–770. doi: 10.1007/s11071-010-9835-y